# Effects of Internal Luminescence and Internal Optics on $V_{oc}$ and $J_{sc}$ of III–V Solar Cells

Myles A. Steiner, John F. Geisz, Iván García, Daniel J. Friedman, Anna Duda, Waldo J. Olavarria, Michelle Young, Darius Kuciauskas, and Sarah R. Kurtz

***Abstract*—For solar cells dominated by radiative recombination, the performance can be significantly enhanced by improving the internal optics. We demonstrate a detailed model for solar cells that calculates the external luminescent efficiency and discuss the relationship between the external and internal luminescence. The model accounts for wavelength-dependent optical properties in each layer, parasitic optical and electrical losses, multiple reflections within the cell, and assumes isotropic internal emission. For single-junction cells, the calculation leads to $V_{oc}$, and for multijunction cells, the calculation leads to the $V_{oc}$ of each junction as well as the luminescent coupling constant. In both cases, the effects of the optics are most prominent in cells with high internal radiative efficiency. Exploiting good material quality and high luminescent coupling, we demonstrate a two-junction nonconcentrator cell with a conversion efficiency of (31.1 ± 0.9)% under the global spectrum.**

***Index Terms*—Luminescence, luminescent coupling, photon recycling, radiative recombination, III–V solar cell.**

## I. Introduction

FOR solar cells dominated by radiative recombination, the open-circuit voltage $V_{oc}$, short-circuit current $J_{sc}$, and ultimately the efficiency can be significantly enhanced by improving the internal optics and by harnessing the energy of the internal luminescence. Internally radiated photons can be directly emitted from the cell, but if confined by good internal reflectors at the front and back of the cell, they can also be reabsorbed with a significant probability. This so-called photon recycling leads to an increase in the equilibrium minority carrier concentration and, therefore, $V_{oc}$. In multijunction cells, the internal luminescence from a particular junction can also be coupled into a lower bandgap junction where it generates photocurrent in addition to the externally generated photocurrent, which shifts the equilibrium $J_{sc}$ and affects the overall performance of the tandem. Both of these phenomena—photon recycling and luminescent coupling—are enhanced by high radiative efficiency and by the tailored geometrical design of the solar cell. In this paper, we extend the ray-optic model of luminescence that we have developed [1] to multijunction cells and use this model to develop and analyze high-efficiency solar cells that exploit a high internal luminescence and good optical properties.

## II. Internal Optics

On thermodynamic grounds, it has been shown [2], [3] that $V_{oc}$ of a solar cell can be expressed as

$$V_{oc} = V_{db} + \frac{kT}{q} \ln(\eta_{ext}) \tag{1}$$

where $V_{db}$ is the value of $V_{oc}$ in the ideal, detailed-balance limit where there are no nonthermodynamic losses, and $\eta_{ext}$ is the external luminescent efficiency, or the fraction of electron–hole pairs that recombine radiatively to yield a photon that ultimately escapes the cell. In real devices, however, there are electrical losses due to nonradiative recombination, and we quantify the fraction of electron–hole pairs that recombine radiatively as the internal luminescent efficiency, $\eta_{int}$. There are also parasitic optical losses due to imperfect reflectances and transmittances. All of these losses are aggregated into $\eta_{ext}$, which represents a loss in voltage and, therefore, conversion efficiency. Consequently, an *increase* in $\eta_{ext}$ indicates an *improvement* in the internal processes of the cell or, equivalently, a decrease in one or more loss mechanisms.

The effect of the internal optics can be clearly demonstrated in a set of double heterostructures (DHs) by measuring the minority carrier lifetime with time-resolved photoluminescence (TRPL). This simple experiment has the advantage that there is no junction or significant doping profile to complicate the carrier dynamics. We grew a set of 16 DHs of $Ga_{0.5}In_{0.5}P$/GaAs/$Ga_{0.5}In_{0.5}P$ on 2°B-miscut (0 0 1) GaAs substrates, with a range of carrier concentrations. We first measured the TRPL decays on the as-grown samples, then removed the GaAs substrates and bonded the epilayers to glass with a transparent low viscosity epoxy and remeasured the TRPL decays. On substrate, the DH is "clad" by air (index of refraction $n = 1$) on one side and GaAs ($n \sim 3.6$) on the other. Bonded to glass, the DH is clad by air on one side and epoxy/glass ($n \sim 1.5$) on the other. Thus, the optical environment has changed. Schematics of the DH samples are shown in Fig. 1(a).

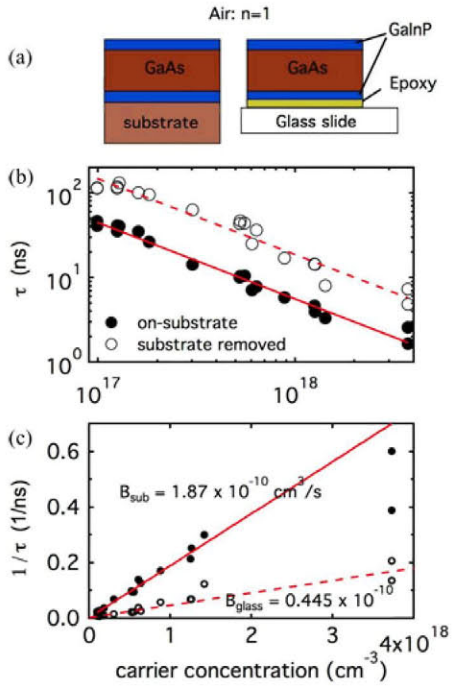


Fig. 1. Minority carrier lifetime of 16 DH samples, as measured by TRPL. (a) Schematics of the samples on-substrate and bonded to glass. (b) Measured lifetime as-grown (solid) and bonded to glass (open). (c) Reciprocal lifetime. The lines show a fit to (2).

Samples were grown by atmospheric pressure metal–organic vapor phase epitaxy. The p-type majority carriers were derived from a triethylzinc source, and the majority carrier concentration was varied from $\sim 1 \times 10^{17}$ to $40 \times 10^{17}$ cm$^{-3}$ by changing the temperature, growth rate, phosphine overpressure, and dopant flow rate. The carrier concentration in the GaAs layer was measured by standard capacitance–voltage ($C$–$V$) methods with a dilute hydrochloric acid electrolyte. Time-correlated single photon counting was used to measure room temperature TRPL decays at 870 nm, with excitation at 630 nm. The average laser power was 0.2 mW, the repetition rate was 1 MHz, and the pulse length was 0.3 ps. The optical-fiber-based TRPL spectrometer is described elsewhere [4]. For all samples, the TRPL was well described by a single exponential decay which enabled a straightforward determination of the lifetime.

Fig. 1(b) shows the measured lifetime as a function of the carrier concentration $N_A$. For both measurement sets, the measured lifetime varies with $N_A$ as $\tau \sim N_A^{-0.9}$ as shown by the solid and dashed lines. Since we expect the radiative lifetime $\tau_R$ to vary with the concentration as $\tau_R = 1/BN_A$, where $B$ is the radiative recombination coefficient, the data indicate that the total recombination is close to the radiative limit. Removing the substrate has the effect of increasing the lifetime by a factor of $\sim$4. In Fig. 1(c), the reciprocal of the lifetime is plotted as a function of the carrier concentration and the data are fit to

$$\frac{1}{\tau} = \frac{1}{\tau_{\mathrm{SRH}}} + BN_A \tag{2}$$

where $\tau_{\mathrm{SRH}}$ is the nonradiative Shockley–Read–Hall lifetime (Auger recombination can be neglected at these doping levels). The coefficient $B$ is found to be $1.87 \times 10^{-10}$ cm$^3$/s for the on-substrate samples and $0.445 \times 10^{-10}$ cm$^3$/s when the substrate was removed. In both cases, $\tau_{\mathrm{SRH}} \sim 2.7 \pm 0.1\mu$s, and for all data points, $\tau \ll \tau_{\mathrm{SRH}}$. Thus, the samples are indeed dominated by radiative recombination, and by removing the substrate, the effective radiative lifetime has increased solely because of the change in the optical environment surrounding the semiconductor. In Section III, we show that these data can be used to quantify $\eta_{\mathrm{int}}$ and confirm that in this case $\eta_{\mathrm{int}} \approx 1$.

As shown in [5], the functional dependence of the radiative lifetime $\tau_R$ can be expressed as

$$\frac{1}{\tau_R} \sim \frac{n_{\mathrm{top}}^2 + n_{\mathrm{bot}}^2}{2n_{\mathrm{sc}}^2} \tag{3}$$

where $n_{\mathrm{top}}$, $n_{\mathrm{bot}}$, and $n_{\mathrm{sc}}$ are the indices of refraction of the top and bottom cladding layers and the semiconductor, respectively. Since the coefficient $B \sim 1/\tau_R$, we calculate the expected ratio of measured coefficients in the radiative limit to be

$$\frac{B_{\mathrm{glass}}}{B_{\mathrm{sub}}} = \frac{(1.5)^2 + 1}{(3.6)^2 + 1} = 0.233 \tag{4}$$

which is in excellent agreement with the measured ratio of 0.238.

## III. Photon Recycling in Single-Junction Solar Cells

The DH experiment illustrates that for optoelectronic devices that are dominated by radiative recombination, the minority carrier lifetime can be significantly enhanced by improving the internal optics of the device. Since the dark current of a solar cell is inversely related to the minority carrier lifetime, we expect the performance of the cell to increase as the lifetime increases.

To understand and predict how the material quality and geometry of the cell affect the performance, we developed a ray-optical model of the external and internal luminescence. The model was described in detail in [1]; here, we summarize the main aspects.

It is useful to think of the solar cell as an optical cavity where photons generated in the absorber layer can reflect multiple times off the two cladding interfaces and possibly interfere with each other. For thick solar cells, it is generally sufficient to treat the cavity with ray optics in which only the intensity of the light varies with location. The optical cavity must have a high absorbance so that most of the incoming light is converted into electron–hole pairs. However, the optical cavity must also manage the internal luminescence: While some of the internally emitted photons will escape out the front of the cell or be reabsorbed parasitically in the cladding layers or in the substrate (if still present), a significant fraction of the photons will be reabsorbed in the absorber layer and reincarnated as new electron–hole pairs.

To escape the cell, an internally emitted photon can escape directly, possibly after bouncing around the cell cavity several times due to the highly reflective cladding surfaces; or it can be reabsorbed, reemitted and then escape; or be reabsorbed again, and so on.

We define $P_{\mathrm{esc}}(\vec{r})$ and $P_{\mathrm{abs}}(\vec{r})$ to be, respectively, the probabilities that a photon emitted at position $\vec{r}$ either escapes directly

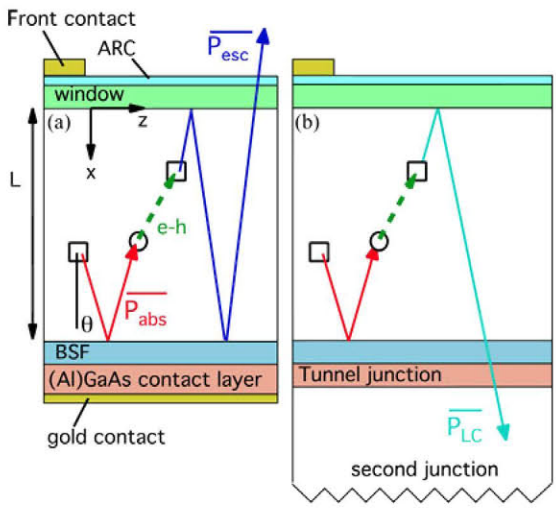


Fig. 2. Schematic of cell geometry and luminescent paths for (a) single-junction and (b) tandem solar cells. The solid lines represent the probabilities $\overline{P_{\rm esc}}$ (dark blue), $\overline{P_{\rm abs}}$ (red) and $\overline{P_{LC}}$ (light blue). The green-dashed line represents electron–hole pair diffusion.

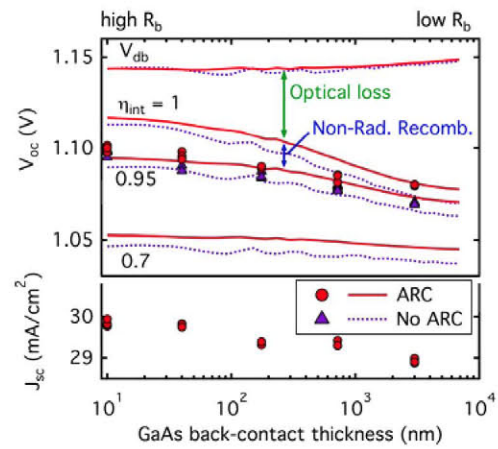


Fig. 3. $V_{\rm oc}$ and $J_{\rm sc}$ for a set of 2-$\mu$m GaAs cells, and modeled $V_{\rm oc}$ curves following (1) and (6)–(8). The top curve shows the detailed balance voltage $V_{\rm db}$. Red points/lines are for AR-coated cells, purple points/lines are for uncoated cells.

or is reabsorbed. Both quantities are already averaged over the spontaneous energy distribution and the uniformly distributed solid angle of internal emission. If $\eta_{\rm int}$ varies with position, then it can be expressed as $\eta_{\rm int}(\vec{r})$, and following the derivation in [1], the external luminescent efficiency is

$$\eta_{\rm ext} = \frac{\int \eta_{\rm int}(\vec{r}) P_{\rm esc}(\vec{r}) d\vec{r}}{1 - \int \eta_{\rm int}(\vec{r}) P_{\rm abs}(\vec{r}) d\vec{r}}. \tag{5}$$

If we assume, however, that for very high quality cells, $\eta_{\rm int}$ is uniformly distributed over the cell volume, then (5) simplifies to

$$\eta_{\rm ext} = \frac{\eta_{\rm int}\overline{P_{\rm esc}}}{1 - \eta_{\rm int}\overline{P_{\rm abs}}} \tag{6}$$

as derived explicitly in [1], where $\overline{P_{\rm esc}}$ and $\overline{P_{\rm abs}}$ now represent energy-, solid-angle-, and volume-averaged probabilities. These quantities are shown schematically in Fig. 2(a). Equation (6) shows that the internal efficiency and the optical-geometrical properties have been effectively separated for high-quality cells. The probabilities can be expressed in (7) and (8), shown at the bottom of the page.

In these expressions, $R_f = R_f(E,\theta), T_f = T_f(E,\theta), R_b = R_b(E,\theta)$, and $T_b = T_b(E,\theta)$ are the effective energy- and angle-dependent Fresnel coefficients for specular reflection and transmission at the front and back interfaces and can be calculated with the transfer matrix method [6] by accounting for the thicknesses and optical coefficients of every layer in the cell; $\alpha = \alpha(E)$ is the energy-dependent absorption coefficient of the absorber layer; $\hat{S}(E)$ is the normalized spontaneous emission distribution of the absorber layer; and $\theta$ is the polar angle shown in Fig 2(a). Notice that the probabilities, and therefore $\eta_{\rm ext}$, do not depend explicitly on the average reflectance at either cladding interface.

To demonstrate the utility of the model, a series of single-junction GaAs cells was grown. The cell geometry is sketched in Fig. 2(a) and consists of an absorber layer of thickness $L$ that is passivated on the front by an AlInP window layer and on the back by a so-called GaInP back-surface field layer (BSF). Behind the BSF layer is an AlGaAs/GaAs contact layer for making Ohmic contact, and behind that is a reflective layer of gold. The front of the cell is covered with an antireflection coating. Details of the fabrication are shown elsewhere [1]. Cells with different absorber layers have the same overall architecture.

Fig. 3 shows the measured $V_{\rm oc}$ for a 2-$\mu$m-thick GaAs cell, with and without an antireflection coating, as a function of the thickness of the absorbing GaAs back-contact layer. Although the primary function of the contact layer is to enable ohmic contact between the electroplated gold and the semiconductor, the layer can also serve a secondary purpose of lowering the overall reflectance by absorbing some of the luminescence, to allow a systematic exploration of the optical effects. In Fig. 3, the average back reflectance decreases from left to right. The data show that $V_{\rm oc}$ decreases by ~20 mV as the contact layer is thickened from 10 nm to 3 $\mu$m, and that $V_{\rm oc}$ increases by

$$\overline{P_{\rm esc}} = \int_0^\infty \hat{S}(E) \int_0^{\pi/2} \frac{T_f}{2\alpha L} \frac{\left(1-e^{-\alpha L/\cos\theta}\right)\left(1+R_b e^{-\alpha L/\cos\theta}\right)}{1 - R_f R_b e^{-2\alpha L/\cos\theta}} \cos\theta \ \sin\theta \ d\theta \ dE \tag{7}$$

and

$$\overline{P_{\rm abs}} = 1 - \int_0^\infty \hat{S}(E) \int_0^{\pi/2} \left\{ \frac{\left(1-e^{-\alpha L/\cos\theta}\right)}{\alpha L} \left(1 - \frac{1}{2}\left(1-e^{-\alpha L/\cos\theta}\right)\left(\frac{R_f + R_b + 2R_f R_b e^{-\alpha L/\cos\theta}}{1 - R_f R_b e^{-2\alpha L/\cos\theta}}\right)\right)\right\} \cos\theta \ \sin\theta \ d\theta \, dE \tag{8}$$

~5 mV when the cell is AR-coated. The cells with the best optics demonstrated conversion efficiencies of (27.8 ± 0.8)% under the global spectrum [1].

The solid lines show the modeled $V_{\rm oc}$ as calculated from (1) and (6)–(8) for different values of $\eta_{\rm int}$. We modeled the external quantum efficiency (EQE) of the cell at each value of the back-contact thickness and then calculated the probabilities $\overline{P_{\rm esc}}$ and $\overline{P_{\rm abs}}$ from the modeled structure. The data are reasonably modeled by $\eta_{\rm int} \sim 0.965$ for both coated and uncoated cells, which is not surprising: the antireflection coating affects the optical cavity properties by changing the front reflectance, but it should not have any effect on the relative recombination rates for an electron–hole pair.

The top curves show the value of $V_{\rm db}$ as calculated from the modeled EQE. $V_{\rm db}$ is an important characteristic of a solar cell and must be calculated for the particular geometry. As the optical cavity changes, by changing the absorber thickness or the back reflectance, for example, the value of $V_{\rm db}$ will also change. The data indicate the general trend that $V_{\rm db}$ increases as the cell absorbance decreases. For these 2-$\mu$m cells, the GaAs absorber becomes less than optically thick, relative to the incident light, as the back reflectance decreases, and therefore, the absorbance also decreases from left to right as can be seen in the $J_{\rm sc}$ data in the lower panel.

Several important conclusions can be drawn from Fig. 3. $V_{\rm oc}$ is clearly more sensitive to the back reflectance in cells of high material quality (i.e., large $\eta_{\rm int}$), as can be seen from the different slopes of the lines with $\eta_{\rm int} = 1$ and 0.7. Conversely, improved material quality has a more pronounced effect on the performance in cells with good optical properties than with poor optical properties. Finally, in this model of a solar cell, the optical and nonradiative recombination losses are separable, as indicated by the vertical arrows. Even for a cell with perfect material quality, $V_{\rm oc} < V_{\rm db}$ because of the parasitic optical losses during the reflection of light at the front and back surfaces.

Fig. 3 also helps address a concern about the broad applicability of the model. The requirement of uniform internal luminescent efficiency implicitly assumes that the solar cell can be described by a single-diode equation at voltages near $V_{\rm oc}$, for if this is not true and a sizeable depletion region (where $\eta_{\rm int} \approx 0$) causes a second term in the diode equation to be significant at voltages near $V_{\rm oc}$, then $\eta_{\rm int}$ can explicitly no longer be uniform. We write the internal luminescent efficiency as

$$\eta_{\rm int} = \frac{U_{\rm rad}}{U_{\rm rad} + \left(U_{nr}^{\rm bulk} + U_{nr}^{\rm dep}\right)} \tag{9}$$

where $U_{\rm rad}$ is the radiative recombination rate, and the total nonradiative recombination rate is separated into contributions from the bulk and depletion regions. If recombination in the depletion region is negligible near $V_{\rm oc}$, then $U_{nr}^{\rm dep} \ll U_{nr}^{\rm bulk}$ and $V_{\rm oc}$ depends on $\eta_{\rm int}$, as shown in Fig. 3; as we have already noted, the internal optics are irrelevant for low values of $\eta_{\rm int}$ which could occur if there are many defect sites within the bulk and $U_{nr}^{\rm bulk}$ is high. If recombination in the depletion region is not negligible near $V_{\rm oc}$, however, then $U_{nr}^{\rm dep} \gg U_{nr}^{\rm bulk}$, the denominator of (9) becomes very large and $\eta_{\rm ext} \approx \eta_{\rm int}\overline{P_{\rm esc}} \to 0$, in which case the optics are again irrelevant. Thus, for cells that are dominated by nonradiative recombination, whether in the bulk or in the depletion region, the influence of the internal optics is negligible and the model may not be particularly useful. For cells that are dominated by radiative recombination, however, the model is very useful and can direct the designer to further improvements by means of the internal optics.

The model can also be used to determine the value of $\eta_{\rm int}$ for the samples in the DH experiment of Fig. 1. We expect the radiative recombination coefficient $B$ to be proportional to the probability that an electron–hole pair is not reincarnated, or $B \sim 1 - \eta_{\rm int}\overline{P_{\rm abs}}$. Based on the layer structure, we calculate $\overline{P_{\rm abs}} = 0.711$ for the sample on-substrate, and $\overline{P_{\rm abs}} = 0.951$ when bonded to glass, a ~33% increase in $\overline{P_{\rm abs}}$. Therefore, using the measured ratio $\frac{B_{\rm glass}}{B_{\rm sub}} = 0.238$, we find $\eta_{\rm int} \approx 0.97$ which is consistent with the measurements on the actual GaAs cells. While DHs are usually used to measure the lifetime of a particular sample or to determine the surface recombination velocity at an interface, this experiment shows that they can also be a valuable test structure to determine $\eta_{\rm int}$ and to evaluate whether the internal optics are good enough to result in a high degree of photon recycling.

## IV. Luminescent Coupling in Tandem Solar Cells

If the back reflector is replaced by a tunnel junction and a second, lower bandgap junction to form a tandem cell, some fraction of the luminescence can couple into the lower bandgap junction, as shown in Fig. 2(b). The probability that photons directly escape out the back of the top junction can be calculated simply by interchanging $R_b \to R_f$ and $T_f \to T_b'$ in expression (7) for $\overline{P_{\rm esc}}$. Care must be taken to only count those photons in the Fresnel coefficient $T_b'$ that are actually absorbed and collected in the lower junction, and not include any photons that escape out the back of the top junction but are absorbed elsewhere; this consideration is indicated by the prime superscript. For high-quality cells where the diffusion length is comparable with the thickness, the collection efficiency is close to unity, and we assume so in the model.

The new quantity $\overline{P_{LC}}$ can be expressed explicitly in (10), shown at the bottom of the page.

Following the same reasoning as for $\eta_{\rm ext}$, the luminescent coupling constant $\eta_{LC}$ can then be defined as

$$\eta_{LC} = \frac{\eta_{\rm int}\overline{P_{LC}}}{1 - \eta_{\rm int}\overline{P_{\rm abs}}}. \tag{11}$$

In a configuration where the tandem cell is current-limited by the bottom junction, the coupling raises the photocurrent of the bottom junction and represents a recovery of photocurrent that

$$\overline{P_{LC}} = \int_0^\infty \hat{S}(E) \int_0^{\pi/2} \frac{T_b'}{2\alpha L} \frac{\left(1 - e^{-\alpha L/\cos\theta}\right)\left(1 + R_f e^{-\alpha L/\cos\theta}\right)}{1 - R_f R_b e^{-2\alpha L/\cos\theta}} \cos\theta \ \sin\theta \ d\theta \ dE. \tag{10}$$

would otherwise be lost if those photons were simply absorbed parasitically; in all configurations, the coupling raises the overall $V_{oc}$ [7]. In general, high coupling will be driven by high $\eta_{int}$ in the top junction and by a minimal degree of parasitic absorption between the junctions, for example, in the tunnel junction layers.

We recently showed a technique [8], [9] to measure the coupling constant, defined there as $\eta_{ij}$ between adjacent junctions $i$ and $j$, based on the measurement of the tandem $J_{sc}$ as the relative intensities on the two (or more) junctions are systematically varied. Using the modeling shown here, we can compare the measured and modeled coupling constants and, more importantly, use the model to design multijunction cells that take advantage of the coupling [10].

In [11], we demonstrated the ability to artificially control the coupling $\eta_{12}$ in a two-junction GaInP/GaAs tandem, by thickening an absorbing $Al_{0.2}Ga_{0.8}$ As layer grown between the two junctions. The data there showed $\eta_{12}$ dropping by a factor of 2, while $\eta_{int}$ for the top junction remained constant. Here, we demonstrate the value of luminescent coupling by varying the thickness of the top junction, to change the externally induced photocurrents on each junction.

Fig. 4(a) shows the EQE for four GaInP/GaAs tandem cells in which the top junction thickness was varied from 0.6 to 1.2 $\mu$m. The bottom junction EQE has been corrected for luminescent coupling [9], [12]. For the three thinnest top junctions, the data show the expected gradual increase in the top junction red response as the junction is thickened, and a corresponding decrease in the bottom junction EQE at those wavelengths. The 1.2-$\mu$m top junction has a red response similar to the 1.0-$\mu$m junction but a diminished blue response which likely indicates that the emitter thickness has exceeded the minority carrier diffusion length. This last cell, therefore, does not quite satisfy the model's assumption of perfect collection efficiency and should be treated with caution, but is included for completeness.

Fig. 4(b) shows the measured coupling constant $\eta_{12}$ which remains approximately constant, with some fluctuation, as the top junction gets thicker. Fig. 4(c) shows the measured values of the externally induced top and bottom photocurrents $J_1^{ext}$ and $J_2^{ext}$ [8], as well as the actual $J_{sc}$ values measured at 1 sun under the G173-global spectrum (1000 W/m$^2$). For thick top junctions, $J_1^{ext}$ exceeds $J_2^{ext}$ by up to 10% and the tandem is clearly bottom-limited. The thickest cell shows a lower value of $J_1^{ext}$ than the 1-$\mu$m cell, again because of the reduced collection efficiency. The actual $J_{sc}$ for the three thickest cells exceeds the limiting external photocurrent $J_2^{ext}$ because of the coupling and is much less sensitive to top junction thickness than is $J_2^{ext}$. As the top junction is thinned to 0.6 $\mu$m, however, the cell crosses over to being slightly top-limited. Under the UV-rich AM0 spectrum (1367 W/m$^2$), the trends are the same but more pronounced.

Without any luminescent coupling, we would expect the decreasing photocurrent to result in a decrease in conversion efficiency, as modeled by the dashed lines in Fig. 4(d). The modeling was adjusted to account for realistic series resistance, but the trends in the model are the most important feature rather than the absolute values. For the global spectrum, the efficiency should peak at a top junction thickness of ~0.7 $\mu$m and for

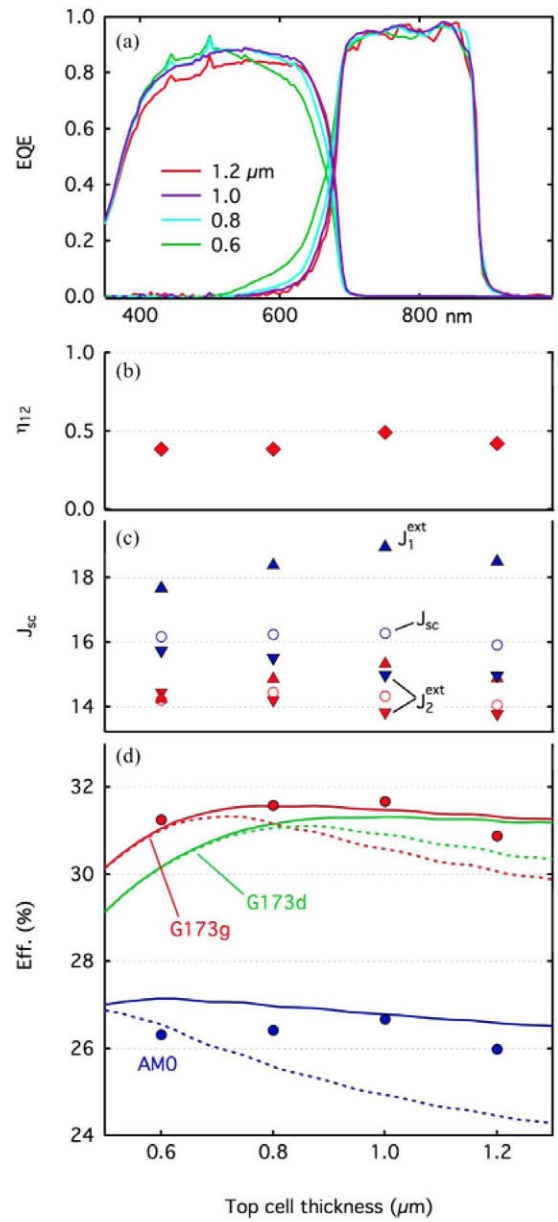


Fig. 4. GaInP/GaAs tandem cells with varied top junction thickness. (a) EQE after correction for luminescent coupling. The top junction thicknesses are indicated in the legend. (b) Measured value of $\eta_{12}$. (c) Measured values of the photocurrents under the G173-global (red) and AM0 (blue) solar spectra. Upward and downward triangles correspond to $J_1^{ext}$ and $J_2^{ext}$, and circles correspond to $J_{sc}$. (d) Conversion efficiency under global, direct and AM0 spectra, as indicated. Points show measured values (for global and AM0), solid lines show modeled values, dashed lines show modeled values with $\eta_{LC} = 0$.

the direct spectrum at ~0.8 $\mu$m. The sensitivity to thickness is more dramatic for the AM0 spectrum. The data, however, show a significantly reduced sensitivity to top junction thickness, as the luminescent coupling has conspired to recover some of the otherwise-lost photocurrent and boost the $J_{sc}$, and thereby increase the efficiency. Indeed, the measured efficiencies under both the global and AM0 spectra are nearly flat despite the large variation in externally induced photocurrents, which indicates that, for terrestrial applications, the cells are well positioned to

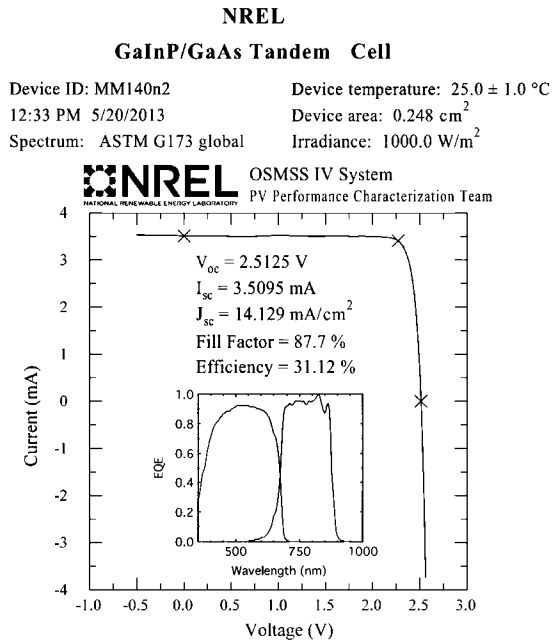


Fig. 5. NREL-certified *I–V* curve for a GaInP/GaAs solar cell, under the AM1.5-G173 global spectrum at 1000 W/m$^2$. The EQE is shown in the inset, corrected for luminescent coupling.

mitigate efficiency loss from spectral variation over the course of operation [7], [13].

Fig. 5 shows an NREL-certified *I–V* curve for a tandem that takes advantage of the concepts discussed here. The cell is bottom-limited with a luminescent coupling constant $\eta_{LC} = 0.56$, driven in large part by the high material quality of the GaInP: Using the model, we calculate $\eta_{\rm int} \sim 80\%$ for the top junction [14]. The diffusion barrier on the n-side of the tunnel junction was $Al_{0.3}Ga_{0.7}As$ with a bandgap of ~1.66 eV, chosen to minimize the absorption of luminescence. The GaAs bottom junction was thinned to 2 $\mu$m and a reflective gold back contact was deposited on an $Al_{0.3}Ga_{07}As$ back-contact layer, also designed to minimize the absorption of luminescence. The front metallization grid was designed for 1-sun intensity, with approximately 2% shadowing. The luminescent coupling measurement of this cell shows the externally induced photocurrents to be $J_1^{\rm ext} = 14.95$ and $J_2^{\rm ext} = 13.55$ mA/cm$^2$, and the equilibrium photocurrents to be $J_1^{\rm equil} = 14.95$ and $J_2^{\rm equil} = 13.98$ mA/cm$^2$: The bottom photocurrent increases by ~3% because of the coupling. $V_{\rm oc}$ of 2.513 V is higher than baseline examples because of the significant photon recycling in the two junctions. The cell had a conversion efficiency of (31.1 ± 0.9)% under the AM1.5-G173 global spectrum at 1000 W/m$^2$, which is the highest demonstrated efficiency for a two-junction 1-sun cell to date.


## Acknowledgment

The authors are grateful for conversations with J. Olson, E. Yablonovitch, C.-S. Ho, R. King, W. McMahon and R. France, and to K. Emery and T. Moriarty for the data in Fig. 5.


## References


[1] M. A. Steiner, J. F. Geisz, I. Garcia, D. J. Friedman, A. Duda, and S. R. Kurtz, "Optical enhancement of the open-circuit voltage in high quality GaAs solar cells," *J. Appl. Phys.*, vol. 113, pp. 123109-1–123109-11, 2013.

[2] U. Rau, "Reciprocity relation between photovoltaic quantum efficiency and electroluminescent emission of solar cells," *Phys. Rev. B*, vol. 76, pp. 085303-1–085303-8, 2007.

[3] O. D. Miller, E. Yablonovitch, and S. R. Kurtz, "Strong internal and external luminescence as solar cells approach the Shockley-Queisser limit," *J. Photovoltaics*, vol. 2, pp. 303–311, 2012.

[4] D. Kuciauskas, J. N. Duenow, J. V. Li, M. R. Young, P. Dippo, and D. H. Levi, "Time resolved photoluminescence spectrometer for thin-film absorber characterization and analysis of TRPL data for CdS/CdTe interface," presented at the 38th IEEE Photovoltaic Spec. Conf., Austin, TX, USA, 2012.

[5] E. Yablonovitch, T. J. Gmitter, and R. Bhat, "Inhibited and enhanced spontaneous emission from optically thin AlGaAs/GaAs double heterostructures," *Phys. Rev. Lett.*, vol. 61, pp. 2546–2549, 1988.

[6] E. Centurioni, "Generalized matrix method for calculation of internal light energy flux in mixed coherent and incoherent multilayers," *Appl. Opt.*, vol. 44, pp. 7532–7539, 2005.

[7] D. J. Friedman, J. F. Geisz, and M. A. Steiner, "Analysis of multijunction solar cell current-voltage characteristics in the presence of luminescent coupling," *J. Photovoltaics*, 2013, to be published.

[8] M. A. Steiner and J. F. Geisz, "Non-linear luminescent coupling in series-connected multijunction solar cells," *Appl. Phys. Lett.*, vol. 100, pp. 251106-1–251106-5, 2012.

[9] M. A. Steiner, J. F. Geisz, T. E. Moriarty, R. M. France, W. E. McMahon, J. M. Olson, S. R. Kurtz, and D. J. Friedman, "Measuring IV curves and subcell photocurrents in the presence of luminescent coupling," *J. Photovoltaics*, vol. 3, pp. 879–887, 2012.

[10] D. J. Friedman, J. F. Geisz, and M. A. Steiner, "Effect of luminescent coupling on the optimal design of multijunction solar cells," *J. Photovoltaics*, 2013, submitted for publication.

[11] M. A. Steiner, J. F. Geisz, I. Garcia, D. J. Friedman, and S. R. Kurtz, "Experimental and modeling analysis of internal luminescence in III-V solar cells," presented at the 9th Int. Conf. Concentrating Photovoltaic Syst., Miyazaki, Japan, 2013.

[12] M. A. Steiner, S. R. Kurtz, J. F. Geisz, W. E. McMahon, and J. M. Olson, "Using phase effects to understand measurements of the quantum efficiency and related luminescent coupling in a multijunction solar cell," *J. Photovoltaics*, vol. 2, pp. 424–433, 2012.

[13] A. S. Brown and M. A. Green, "Radiative coupling as a means to reduce spectral mismatch in monolithic tandem solar cell stacks—Theoretical considerations," in *Proc. 29th IEEE Photovoltaic Spec. Conf.*, New Orleans, LA, USA, 2002, pp. 868–871.

[14] J. F. Geisz, M. A. Steiner, I. García, S. R. Kurtz, and D. J. Friedman, "Enhanced external radiative efficiency for 20.8% efficient single-junction GaInP solar cells," *Appl. Phys. Lett.*, vol. 103, pp. 041118-1–041118-5, 2013.


Authors' photographs and biographies not available at the time of publication.